CRYSTAL GROWTH & DESIGN

Article

pubs.acs.org/crystal

Heat-Induced Phase Transformation of Three-Dimensional $Nb_3O_7(OH)$ Superstructures: Effect of Atmosphere and Electron Beam

Sophia B. Betzler,[†,‡] Tristan Harzer,[⊥] Jim Ciston,[§] Ulrich Dahmen,[§] Gerhard Dehm,[⊥] and Christina Scheu*[,⊥,‡]

[†]Department of Chemistry and Center for NanoScience, Ludwig-Maximilians-University, Butenandtstraße 11, 81377 Munich, Germany

[‡]Nanosystems Initiative Munich, Schellingstraße 4, 80799 Munich, Germany

[⊥]Max-Planck-Institut für Eisenforschung GmbH, Max-Planck-Straße 1, 40237 Düsseldorf, Germany

[§]National Center for Electron Microscopy, Molecular Foundry, Lawrence Berkeley National Laboratory, One Cyclotron Road, Berkeley, California 94720, United States

Supporting Information

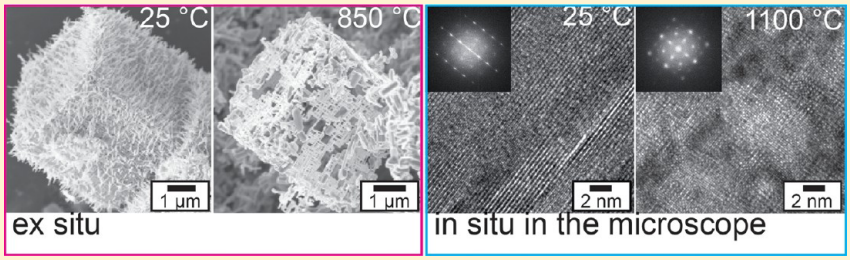

ABSTRACT: Nanostructured niobium oxides and hydroxides are potential candidates for photochemical applications due to their excellent optical and electronic properties. In the present work the thermal stability of $Nb_3O_7(OH)$ superstructures prepared by a simple hydrothermal approach is investigated at the atomic scale. Transmission electron microscopy and electron energy-loss spectroscopy provide insights into the phase transformation occurring at elevated temperatures and probe the effect of the atmospheric conditions. In the presence of oxygen, H_2O is released from the crystal at temperatures above 500 °C, and the crystallographic structure changes to H-Nb_2O_5. In addition to the high thermal stability of $Nb_3O_7(OH)$, the morphology was found to be stable, and first changes in the form of a merging of nanowires are not observed until 850 °C. Under reducing conditions in a transmission electron microscope and during electron beam bombardment, an oxygen-deficient phase is formed at temperatures above 750 °C. This transformation starts with the formation of defects in the crystal lattice at 450 °C and goes along with the formation of pores in the nanowires which accommodate the volume differences of the two crystal phases.

INTRODUCTION

Many different polymorphs are reported for niobium pentoxide, with monoclinic H-Nb_2O_5 being the thermodynamically stable high-temperature phase.[1,2] This phase is observed after calcination of amorphous Nb_2O_5 at 1200 °C via the intermediate formation of T-Nb_2O_5[3] (T > 600 °C) and M-Nb_2O_5[4] (T > 1000 °C).[5] Starting from Nb(IV)O_2, an alternative heat induced transformation pathway to H-Nb_2O_5 occurs with orthorhombic L-Nb_2O_5 forming as intermediate phase which transforms into H-Nb_2O_5 at 850−900 °C.[6] Other polymorphs include orthorhombic G-Nb_2O_5,[7] monoclinic R-Nb_2O_5,[8] and monoclinic zeta-Nb_2O_5.[9] Most polymorphs are characterized by a common structure element as their crystal structures contain edge- and corner-sharing NbO_6 octahedra. In addition to stoichiometric phases, several phases with oxygen deficiency such as monoclinic $Nb_{12}O_{29}$[10] and $Nb_{22}O_{54}$ exist.[11]

Niobium pentoxide can be applied successfully as photocatalyst,[12−16] photodetector,[15] electrode material for photoelectrochemical water splitting[17] and in dye-sensitized solar cells.[18−21] Recently another class of niobium oxides, $Nb_3O_7(OH)$[22], has attracted attention as very promising photochemical properties are discovered for this phase,[23−28] and its performance as electrode material in dye-sensitized solar cells exceeds Nb_2O_5.[23] Both orthorhombic $Nb_3O_7(OH)$ (a = 20.74 Å, b = 3.823 Å, c = 3.926 Å)[22] and monoclinic H-Nb_2O_5 (a = 21.153 Å, b = 3.8233 Å, c = 19.356 Å, β = 119.80°)[3] consist of blocks of corner-sharing NbO_6 octahedra. This structural motif facilitates the phase transformation of $Nb_3O_7(OH)$ to H-Nb_2O_5 as shown by X-ray diffraction (XRD) studies.[23,28] In general, all phase transformations are characterized by their thermodynamic (temperature and pressure) and kinetic properties (heating rate).[29] In situ experiments[30] performed in the electron microscope have

Received: March 9, 2016
Revised: June 10, 2016
Published: June 27, 2016

DOI: 10.1021/acs.cgd.6b00386
Cryst. Growth Des. 2016, 16, 4309−4317

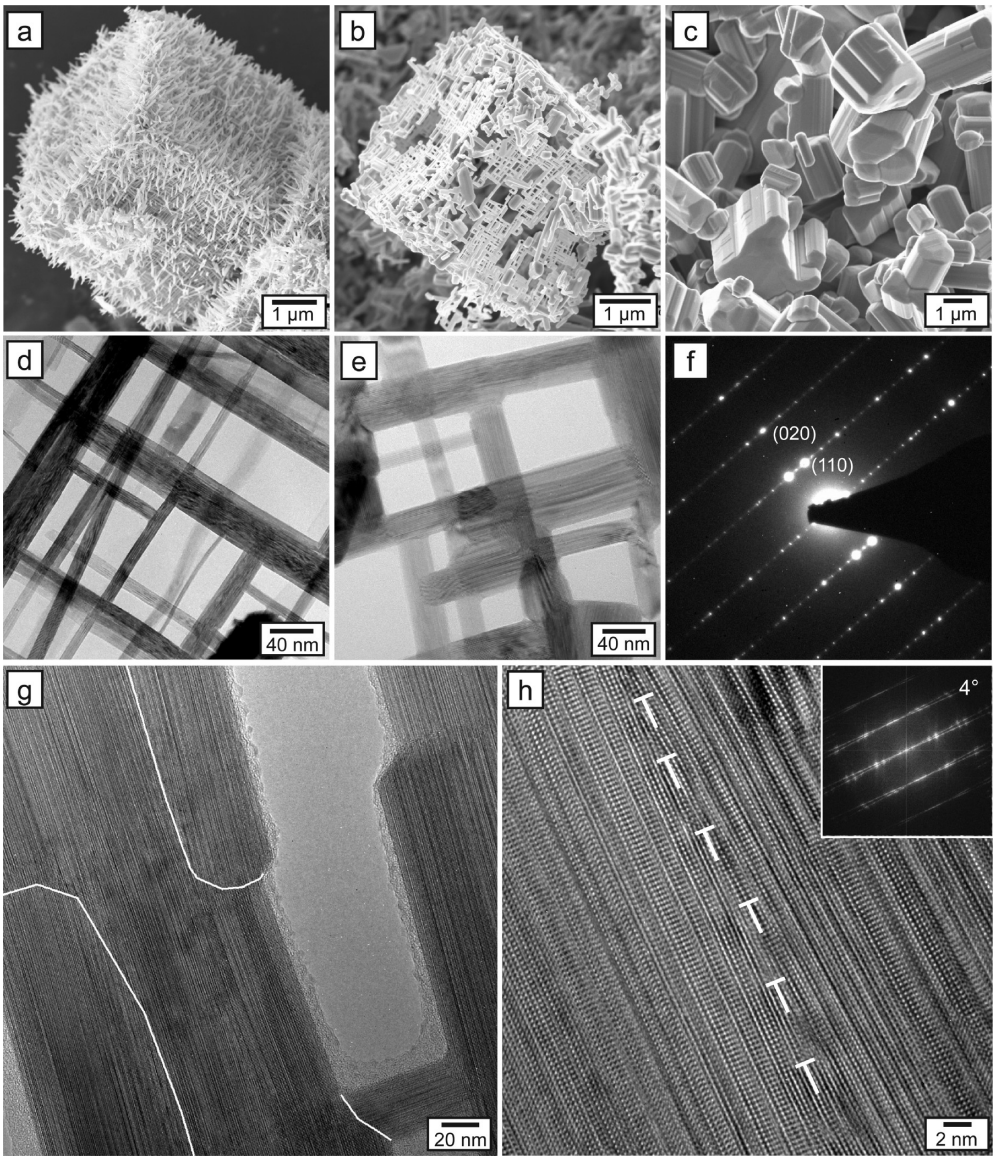

Figure 1. Electron micrographs of samples heated ex situ under ambient conditions. (a) SEM image of the $Nb_3O_7(OH)$ superstructure before the calcination and after the calcination at 850 °C (b) and 1200 °C (c). (d) TEM image of the network consisting of the $Nb_3O_7(OH)$ nanowires before calcination. (e) TEM image of the nanowire network obtained after calcination at 850 °C. The electron diffraction pattern recorded for one nanocrystal in the [001] zone axis is shown in (f). (g) High resolution TEM (HRTEM) image of an area which shows that the nanowires merged to form larger crystals during calcination at 850 °C. The white lines indicate individual grains. (h) Magnified view of the boundary between two nanowires grown together. A miss-tilt of 4° also visible in the fast Fourier transformation (FFT) is compensated by dislocations (highlighted with white lines) arranged in a small angle grain boundary (SAGB).

been demonstrated to give insight into the phenomena occurring during heating for numerous materials including silver,[31] Al_2O_3,[32,33] anatase TiO_2[34] and Al−Si alloy nanoparticles.[35] However, the conditions inside an electron microscope differ from ex situ laboratory synthesis conditions and often result in a reducing environment.[36−38] This is especially interesting in the case of metal oxides with a covalent component in their bonding as they are known for their ability to accommodate slight reduction by crystallographic shear.[39]

In the present work, the annealing behavior of complex three-dimensional (3D) hierarchical $Nb_3O_7(OH)$ superstructures is investigated. They are fabricated by a hydrothermal synthesis strategy[25] and consist of highly ordered nanowire networks. The superstructures are fully crystalline, phase-pure, and have a large surface area, which are beneficial properties for photocatalysts and photoelectrodes.[25] The thermal stability of the morphology and crystal structure of nanostructures is crucial for their application in functional devices. In this work, the heat induced phase transformation of $Nb_3O_7(OH)$ to H-Nb_2O_5 and the effect of annealing on the morphology of the superstructures are studied at the atomic scale as a function of pressure and atmosphere. This is important as some niobium oxide polymorphs are reported to tolerate large deviation from stoichiometry.[11,40,41] In situ experiments carried out in a transmission electron microscope (TEM) are furthermore used to directly observe atomic scale phenomena.

RESULTS AND DISCUSSION

Ex Situ Studies of the Phase Transformation at Ambient Conditions. Figure 1a shows a scanning electron

DOI: 10.1021/acs.cgd.6b00386
Cryst. Growth Des. 2016, 16, 4309−4317

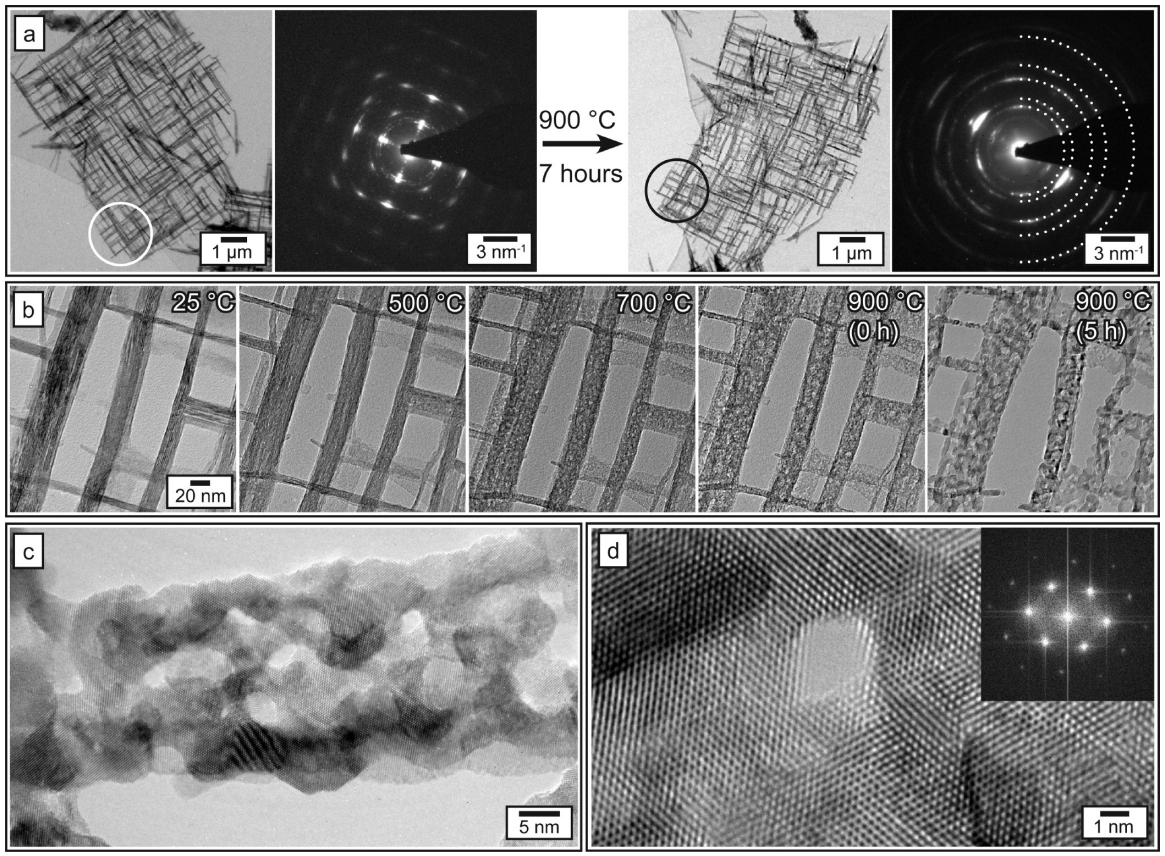

Figure 2. In situ TEM heating experiments which shows the effect of heat and electron bombardment on the structure of nanowire networks. (a) Bright field (BF) images and electron diffraction pattern of the investigated network before and after the heating experiment. (b) BF images recorded during the in situ heating experiment. (c) HRTEM image acquired of one nanowire of the investigated network after the in situ experiment. (d) Close-up view of one region with a pore. The inset shows the FFT pattern calculated of the respective HRTEM image.

microscopy (SEM) image of the 3D hierarchical $Nb_3O_7(OH)$ superstructures investigated in this study. These superstructures were calcined at ambient conditions in the presence of oxygen and analyzed by ex situ XRD and electron microscopy after cooling down to room temperature. XRD reveals changes of the crystallographic structure for an annealing temperature of 500 °C. First a broadening of the reflection at $2\theta_B = 23.6°$ occurs, which coincides with a decrease of the intensity of the (001) reflection of $Nb_3O_7(OH)$ ($2\theta_B = 22.5°$) (see Supporting Information (SI), Figure S1). For a temperature of 850 °C broad reflections are observed as well, which become more pronounced for the sample obtained from calcination at 1200 °C. The comparison with literature[1,2] shows that the reflections of the sample calcined at 1200 °C perfectly match H-Nb_2O_5 (see SI, Figure S2). High resolution imaging performed in the TEM reveals the presence of both crystal phases ($Nb_3O_7(OH)$ and H-Nb_2O_5) in the sample calcined at 600 °C. Hence, an overlap of the strong reflections of H-Nb_2O_5 at 23.8° ((1 1 0), (1 $\bar{1}$ 1)) and 23.9° ((0 1 1)) with the reflections of $Nb_3O_7(OH)$ are responsible for the broadening of the reflections observed in the respective XRD pattern. At the same time SEM images show that the morphology of the superstructures is preserved up to 850 °C (Figure 1b). This is related to the conservation of large parts of the original nanowire networks as obvious from bright field (BF) TEM images (Figure 1d,e). A comparison of the networks before and after calcination at 850 °C reveals that the nanowire arrangement is preserved, while the size of the single wires increases. The electron diffraction pattern acquired for a single nanocrystal of the 850 °C sample confirms that they possess the H-Nb_2O_5 crystal structure with the long dimension being parallel to the [010] direction (see Figure 1f and SI, Figure S3). The H-Nb_2O_5 nanowires show regions with slightly tilted (2–4°) {$\bar{1}$ 0 1} lattice planes as determined from analysis of the fast Fourier transformation (FFT). This deviation is compensated by the formation of small-angle grain boundaries (SAGBs) consisting of edge dislocations with a spacing of $D = 5.8 \pm 1.3$ nm (Figure 1h).

The findings of the TEM investigations indicate a merging of crystallites during the phase transformation, which results in larger nanocrystals and suggests that Ostwald ripening occurs (Figure 1g). This hypothesis is strengthened by the observation of increased crystal sizes for a higher calcination temperature of 1200 °C as indicated by sharp reflections in the XRD (see SI, Figure S2). The large crystal size achieved at 1200 °C is also visible in SEM micrographs (Figure 1c), which in addition show that the superstructures have collapsed into individual large and compact H-Nb_2O_5 crystals. TEM images reveal the compact nature of these single crystals, and electron diffraction experiments indicate the presence of (1 0 $\bar{1}$) twins in the H-Nb_2O_5 crystal lattice. We propose that these twins form during the merging of small nanocrystals as a result of stress or growth twins (see SI, Figure S3). The observation of these twins is in accordance with the literature which describes the (1 0 $\bar{1}$) twin boundary as the only permitted twin boundary in the block structure of H-Nb_2O_5.[42]

DOI: 10.1021/acs.cgd.6b00386
Cryst. Growth Des. 2016, 16, 4309–4317

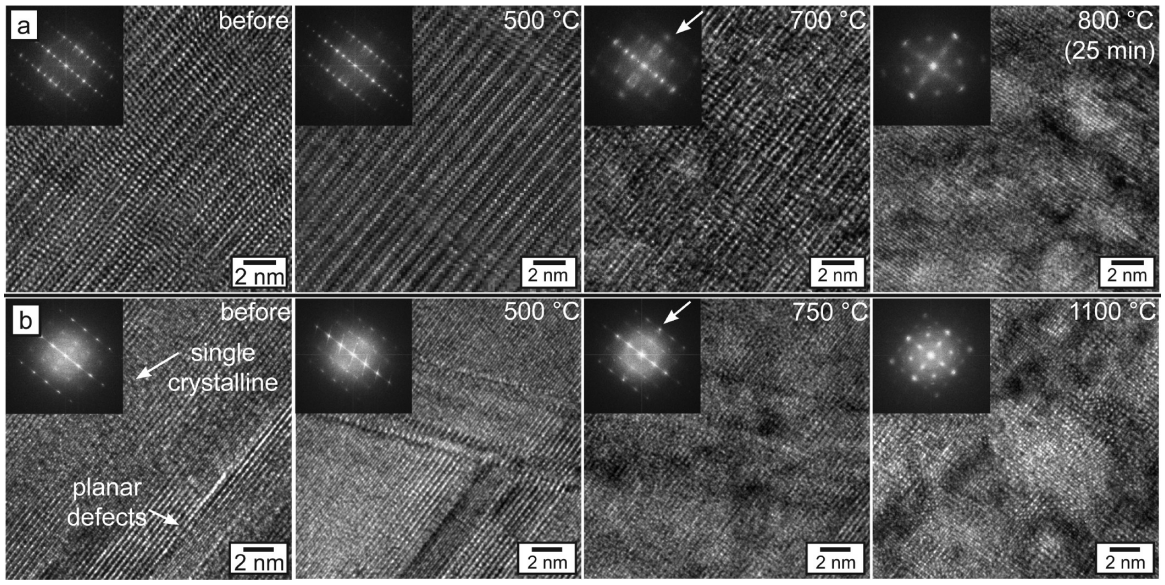

Figure 3. HRTEM images detected during the in situ TEM heating experiments. (a) Screen shots of a movie recorded for a nanowire in [001] viewing direction at different temperatures. (b) Images recorded during an in situ experiment starting from a nanowire in [100] orientation.

The investigation indicates that surprisingly high temperatures are required to remove water from the crystal lattice of $Nb_3O_7(OH)$ to form H-Nb_2O_5 according to the following equation:

$$2Nb_3O_7(OH) \xrightarrow[1\ bar]{\Delta T} 3Nb_2O_5 + H_2O$$

In contrast to a recent study which reported a temperature of 450 °C to suffice for complete transformation of $Nb_3O_7(OH)$ to H-Nb_2O_5,[28] temperatures above 600 °C are required for complete phase transformation of the $Nb_3O_7(OH)$ superstructures investigated in the present work. Furthermore, we apply in-depth TEM analysis, and by this a high thermal stability of both crystal structure and morphology is proven. In situ investigations which allow us to directly observe the phase transformation at the atomic scale are performed under reducing conditions in the TEM as described in the following.

In Situ TEM Investigation of Phase Transformation in Reducing Atmosphere. The size of the 3D hierarchical $Nb_3O_7(OH)$ superstructures (see Figure 1a) necessitates the investigation of fragments of nanowire networks or single nanowires with TEM. The high degree of ordering within the large-scale nanowire networks (see Figure 1d and 2a) is apparent from electron diffraction patterns which exhibit distinct reflections typical for single crystals.[25] The effect of heat on the structure of one whole network was monitored in the course of 300 min at 900 °C with images recorded every 15 min (see Figure 2b). To reduce possible electron beam induced radiation damage (acceleration voltage was 300 kV), the beam was moved to a neighboring area in between the measurements (detailed description of the experiment see SI, Table S1). No changes are observed for temperatures below 500 °C followed by the formation of a substructure in the nanowires (at 700 °C). This structure becomes more pronounced at 900 °C at which point nanoscale pores develop within the nanowires. These pores are surrounded by small nanocrystals. The shape of the pores changes during the first 135 min at 900 °C. Afterward primarily a bending of the nanowires and only slight changes of the nanocrystalline structure are observed (see Movie 1). The comparison of electron diffraction patterns from the investigated region before and after the experiment shows that the long-range ordering within the network is lost (Figure 2a). Figure 2c shows the formation of small nanocrystals which surround the pores. HR TEM images recorded after the heating experiment show that all nanocrystals within the pristine nanowire have the same crystal orientation (Figure 2d). Although these nanocrystals are aligned along the same zone axis they are slightly rotated relative to each other leading to a moiré pattern visible in the HRTEM image. FFT analysis shows that they possess a different crystal structure than the mother compound which cannot definitely be assigned to one specific niobium oxide phase reported in the literature.

In contrast to observations for the $Ni(OH)_2/NiO$ system[43] no changes of the nanowire width are found for the $Nb_3O_7(OH)$ nanowire networks in our in situ study (see SI, Figure S4). It is important to note, that despite the pore formation, a high thermal stability (no changes up to 500 °C) of the nanowire network is also observed under reducing conditions (Figure 2b).

To directly follow the formation of the pores and nanocrystals in situ TEM heating experiments were also conducted at higher magnification for single nanowires oriented parallel to the [0 0 1] (Figure 3a) and [1 0 0] (Figure 3b) direction (the [0 1 0] direction cannot be investigated as it is the growth direction of the nanowires[23,25]). In this case, beam damage was not reduced by moving respective nanowires out of the electron beam but by lowering the accelerating voltage to 200 kV. The crystal lattice of $Nb_3O_7(OH)$ nanowires is not defect free but contains planar defects parallel to the (0 0 1) lattice planes visible in the [1 0 0] viewing direction (Figure 4c). The investigations were performed for regions at the interface between defective and defect-free crystal lattices since the largest changes were expected here. First changes of the crystal lattice occur in the form of additional defects in the temperature range between 400 and 500 °C, and a shift of the atomic position by 1/2 [0 0 1] of every third lattice plane is observed (Figure 4d,e). The dislocations leading to the atomic displacements of 1/2 [0 0 1] originate at the planar defect (Figure 3b) and move through the single crystalline region

DOI: 10.1021/acs.cgd.6b00386
Cryst. Growth Des. 2016, 16, 4309−4317

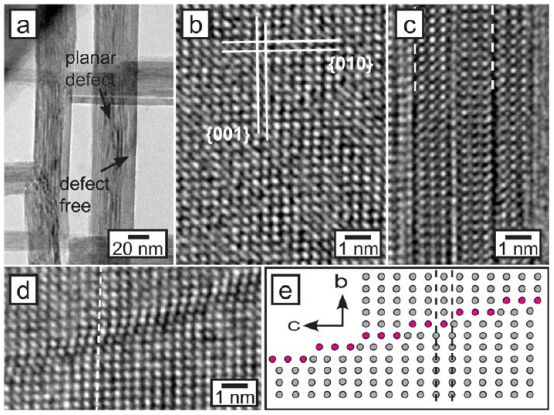

Figure 4. TEM images of the crystal structure of a nanowire in [100] orientation showing a defect-free area and the planar defects parallel to the (001) lattice planes. (a) Overview of one nanowire. (b) Close-up view of a defect-free region; (c) magnified view of the planar defects present in the crystal lattice. (d) HRTEM image of the defects which result from dislocations which move through the crystal lattice at 450 °C. (e) Schematic illustration of the defect structure.

toward the surface of the nanowire with a speed of 5.9 ± 1.3 nm/min at 450 °C (see Movie 2). The dislocations form to relieve strain[44−46] and are believed to initiate the phase transformation which proceeds in the [0 0 1] direction. This agrees well with the reported observation that the phase transformation from $Nb_3O_7(OH)$ to H-Nb_2O_5 likewise happens via crystal deformation along the *z*-direction.[28] At a temperature of 650−750 °C first slight distortions of the crystal lattice cause a blurriness in the FFT pattern and frame the beginning pore formation. With increasing temperatures these pores become more pronounced which coincides with the beginning of a phase transformation as obvious from the FFT pattern. The phase transformation proceeds with ongoing heating time and so does the formation of the pores which increase in size. As soon as the phase transformation is completed, only minor changes of the pore structure are observed and their sizes remain constant (see SI, Figure S5). The formation of pores can be provoked directly at a heating temperature of 900 °C by moving the electron beam to a new network which had not been illuminated before (see Movie 3). In principle several reasons for this pore formation are conceivable. They could form to compensate the volume change occurring during the phase transformation,[43] due to a movement and agglomeration of defects resulting in Kirkendall voids[47,48] or be caused by electron beam damage effects which destroy bonds and remove preferentially one atomic species (e.g., oxygen) from the crystal.[36−38] Of these, the volume change has been shown to be the most likely explanation for numerous decomposition reactions of this type.[43,49] Many such reactions are found to be topotactic and pseudomorphic; i.e., they maintain crystallographic alignment of the parent and product lattices and leave the external shape of the structure largely unchanged. This implies that the volume difference must be accommodated by internal pores. These pores only form when the sample has reached 500 °C, and no changes of the nanowire morphology are observed during electron bombardment at lower temperatures (see Movie 4). Similar pores were observed for Nb_2O_5, but other than that found for $Nb_3O_7(OH)$ in this work the pore formation in Nb_2O_5 is associated with a phase transformation that can be initiated by electron irradiation at room temperature.[37] The study assumes a reduction of Nb_2O_5 by the electron irradiation but could not match the observed *d*-values to a known crystal phase. At temperatures of 1200 °C we find a rapid merging of the initial nanowires via oriented attachment and coarsening under strong crystalline anisotropy (see Movie 5). FFT patterns calculated from HRTEM images acquired at 800 °C (Figure 3a) and 1000 °C (Figure 3b) are found to be different from the parent phase. The pattern of the nanowires illuminated during the experiment differ dependent on the starting orientation of the nanowire (see SI, Figure S6). Neither of these patterns fit to the H-Nb_2O_5 or $Nb_3O_7(OH)$ crystal phase, and the phase variety of niobium oxide and its ability to accommodate reduction by crystallographic shear complicate the phase identification (the determined *d*-values are listed in SI, Table S2).[11,40,41,50]

To address the question of the effect of the electron beam irradiation on the phase transformation further nanowires and networks which had not been illuminated during the in situ heating experiment are analyzed after being cooled down to room temperature. The investigation shows that in the absence of the electron beam a minimum temperature of 900 °C is required to initiate a phase transformation. In that case the networks likewise retain their morphology. Other than in the presence of the electron beam no pore formation is visible, but instead the transformation starts with the formation of small nanograins in the initial nanowires. It appears that these nanograins merge in the course of the recrystallization to form larger single crystals (see SI, Figure S7). It is important to note that at 900 °C not all nanowires have phase transformed, and many preserve the $Nb_3O_7(OH)$ crystal structure. However, after calcination at 1200 °C all nanowires appear to be transformed into a crystal phase which is different from the mother compound or H-Nb_2O_5 and besides *d*-values of 1.9 and 3.2 Å a *d*-value of 14.2 Å is found (Figure 5a,b and SI, Table S2). The large *d*-spacing is solely observed for a few phases which are M-Nb_2O_5 ($d_{(110)}$ = 14.5 Å),[4] T-Nb_2O_5 ($d_{(020)}$ = 14.6 Å)[3] and L-Nb_2O_5 ($d_{(020)}$ = 14.7 Å).[6]

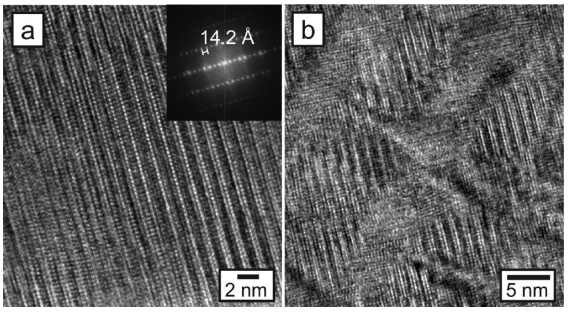

Figure 5. HRTEM images of two nanowires, which were heated in situ to 950 °C in the absence of the electron beam. Panel (a) shows a single crystalline region; the FFT yields a *d*-spacing of 14.2 Å, which does not match $Nb_3O_7(OH)$ and H-Nb_2O_5. A region composed of different crystal orientations which merged during the recrystallization is visible in the HRTEM image displayed in (b).

Electron Energy-Loss Spectroscopy Analysis of the Different Samples. The reducing atmosphere in a TEM and the known sensitivity of niobium oxide to be reduced by the electron beam suggest the removal of oxygen during the in situ TEM experiments, thus reducing the oxidation state of niobium. Therefore, electron energy-loss spectroscopy (EELS) is applied to determine the oxidation state by analyzing the energy-loss near-edge fine structure (ELNES) of the O−K

DOI: 10.1021/acs.cgd.6b00386
Cryst. Growth Des. 2016, 16, 4309−4317

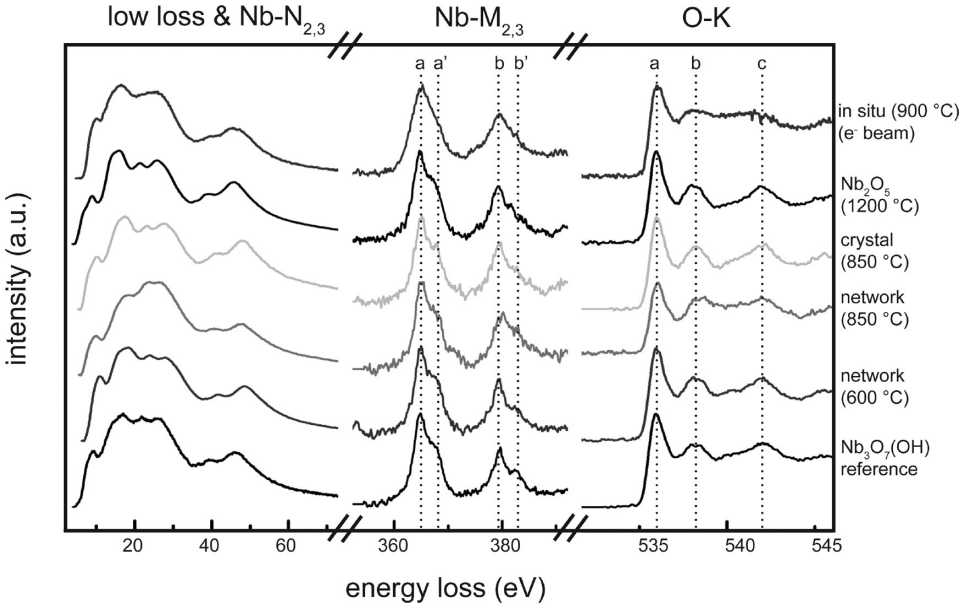

Figure 6. EEL spectra recorded for samples obtained from different heat treatments. Different samples were investigated: One $Nb_3O_7(OH)$ nanowire network as reference as well as networks calcined ex situ at 600 and 850 °C. Furthermore, single nanowires observed after calcination at 850 and 1200 °C were analyzed in addition to the nanowire network which was heated in situ to temperatures of 900 °C in the presence of the electron beam.

Table 1. EELS Data Recorded for the Sample Calcined at Different Temperatures Ex Situ and in Situ in the Presence of the Electron Beam[a]

	Nb-$M_{3,4}$		O−K edge		
sample	*a* (eV)	*b* (eV)	*a* (eV)	*b* (eV)	*c* (eV)
$Nb_3O_7(OH)$ reference	1.5 ± 0.1	16.1 ± 0.2	1.1 ± 0.1	5.6 ± 0.1	13.2 ± 0.2
$Nb_3O_7(OH)$ 600 °C	1.4 ± 0.2	16.0 ± 0.1	1.1 ± 0.1	5.4 ± 0.1	13.0 ± 0.1
network 850 °C	1.4 ± 0.1	16.0 ± 0.1	1.0 ± 0.1	5.3 ± 0.1	13.0 ± 0.1
crystal 850 °C	1.5 ± 0.2	16.2 ± 0.4	1.1 ± 0.1	5.3 ± 0.1	13.1 ± 0.1
Nb_2O_5 (1200 °C-sample)	1.5 ± 0.1	16.1 ± 0.1	1.0 ± 0.1	5.3 ± 0.1	13.1 ± 0.1
in situ network with e-beam	2.2 ± 0.1	16.5 ± 0.4	1.1 ± 0.1	5.0 ± 0.1	-

[a]The peak positions are given relative to the onset of the respective edge which was set to 365 eV for the Nb-$M_{2,3}$ and 532 eV for the O−K edge.

and Nb-$M_{2,3}$ edge and by quantitative determination of the niobium-to-oxygen ratio.

The ELNES of element specific edges in EEL spectra yields a deeper understanding of the oxidation state and local surrounding of the elements in the crystals. EELS data were recorded with an energy resolution of 0.3−0.4 eV (dispersion 0.07 eV) for $Nb_3O_7(OH)$, $Nb_3O_7(OH)$ calcined at 600 and 850 °C and H-Nb_2O_5. The H-Nb_2O_5 phase was obtained via calcination of $Nb_3O_7(OH)$ at 1200 °C. In addition, ELNES data were recorded at the nanowire network heated in situ in the TEM in the presence of the electron beam at 900 °C (Figure 6 and Table 1). The low-loss region which contains the plasmon peak and single valence loss excitations is characterized by four main features with additional shoulders and is very similar for all samples (Figure 6). Slight deviations between the different samples are most likely caused by carbon contamination and thickness variation. In thick samples multiple scattering events can occur, yielding altered ELNES features.[51] However, the low loss region for the different samples do not show any sign of a second plasmon, and as such the different ELNES features discussed below stem from changes in the oxidation state.

The Nb-$M_{2,3}$ edge with an edge onset at around 365 eV results from the transition of electrons of the Nb-3*p* states to unoccupied Nb-4*d*/Nb-5*s* states and is characterized by two white lines. The energy difference between M_2 (*b*) and M_3 (*a*) originates from the spin−orbital splitting of $3p_{1/2}$ and $3p_{3/2}$ orbitals. The M_2 and M_3 difference is 14.6 ± 0.1 eV for $Nb_3O_7(OH)$ and the ex situ heated samples, while a slightly decreased splitting is observed for the sample heated in situ (14.1 ± 0.2 eV) (see Table 1). The ELNES of the Nb-$M_{2,3}$ edges show high energy loss shoulders (*a*′, *b*′) for all samples (ex situ heated samples, H-Nb_2O_5 and $Nb_3O_7(OH)$) except the one heated in situ in the presence of the electron beam. These high-energy loss shoulders are characteristic for pentavalent niobium, while the double peak structure becomes less pronounced for Nb(IV)O_2 and vanishes for Nb(II)O.[52,53] Hence, the observed ELNES of the Nb-$M_{2,3}$ edges proposes the presence of pentavalent niobium in the samples heated ex situ as well as H-Nb_2O_5 and $Nb_3O_7(OH)$. In contrast, the ELNES of the sample heated in situ in the presence of the electron beam indicates the presence of Nb(IV) or Nb(II) in the crystal lattice.

The ELNES of the O−K edge is characterized by three dominant features (*a*, *b*, *c*). The splitting of peak *a* and *b* can serve as a fingerprint for the oxidation state.[53] It is 4.3 ± 0.1 eV for the samples heated ex situ, while it decreases to 3.8 ± 0.1 eV for the sample heated in situ in the microscope. The former

DOI: 10.1021/acs.cgd.6b00386
Cryst. Growth Des. 2016, 16, 4309−4317

values agree well with the ones reported for Nb_2O_5 (4.3 eV[53]), while the latter value indicates a decrease of the niobium oxidation state for the sample heated in situ as a value of 3.5 eV was reported for NbO.[53] The high similarity between $Nb_3O_7(OH)$ and H-Nb_2O_5 is related to the fact that both crystal structures are based on identical structure units. In this regard, the ELNES of the Nb-$M_{2,3}$ as well as the O−K edge indicate a reduction of the niobium oxidation state due to the combination of electron irradiation and the absence of oxygen. The niobium-to-oxygen (N_{Nb}/N_O) ratio of these samples was quantified based on the intensity of the respective edges $I_{O/Nb}$ using the following equation.[51]

$$\frac{N_{Nb}}{N_O} = \frac{I_{Nb}}{I_O}\frac{\sigma_O}{\sigma_{Nb}}$$

Here σ_O and σ_{Nb} are the inelastic cross-section of the O-K and the Nb-$M_{2,3}$ edge, respectively. For $Nb_3O_7(OH)$ a σ_{Nb}/σ_O-factor of 0.86 and for Nb_2O_5 a factor of 0.76 were determined empirically based on the reference sample and H-Nb_2O_5 (1200 °C sample). These factors are used to determine the Nb−O ratio of the sample heated in situ in the microscope in the presence of the electron beam. The Nb−O ratio determined using the cross-section factor (σ_{Nb}/σ_O = 0.76) for $Nb_3O_7(OH)$ is 0.67, while a value of 0.59 was calculated using the σ_{Nb}/σ_O of Nb_2O_5. The values are higher than the ones of $Nb_3O_7(OH)$ (N_{Nb}/N_O = 0.38) and Nb_2O_5 (N_{Nb}/N_O = 0.4) indicating a lower amount of oxygen. These findings coincide with the altered ELNES of the Nb-$M_{2,3}$ and O-K edge discovered for the sample heated in situ in the microscope proving the removal of oxygen from the crystal structure of the sample due to the combination of heat and reducing condition.

CONCLUSION

This study investigates the effect of heat on the morphology and crystal structure of 3D hierarchical $Nb_3O_7(OH)$ superstructures at different atmospheric conditions. These superstructures consist of highly ordered nanowire networks. In the presence of oxygen a transformation of $Nb_3O_7(OH)$ to H-Nb_2O_5 is initiated at temperatures above 500 °C, and the presence of both crystal phases is observed for a sample calcined at 600 °C. At the same time, the morphology of the nanowire networks and with that of the superstructures is preserved up to 850 °C, despite the merging of the nanowires which goes along with phase transformation. This merging is facilitated by SAGBs which form to compensate slight tilting of crystal domains.

The high thermal stability of the nanowire networks is confirmed by in situ investigation in the TEM. However, the reducing condition in the electron microscope has a strong effect on the phase transformation. Prior to the phase transformation, defects form in the single crystalline region of the nanowires at 450 °C. These defects move through the crystal to its surface starting from planar defects which are characteristic for hydrothermally grown $Nb_3O_7(OH)$ nanowires. The presence of the electron beam during the heating experiment features the formation of an oxygen-deficient niobium oxide crystal phase for temperatures above 800 °C. The volume difference between the two crystal phases is compensated by the formation of pores which is observed at temperatures above 700 °C. Solely the presence of the electron beam does not suffice to initiate this pore formation, but at least a temperature of 500 °C is required as well. However, no pores are observed for heating experiments performed in situ in the absence of the electron beam and aside from that under this condition the phase transformation also happens at higher temperatures of 900 °C.

The present study indicates that oxygen has a strong effect on the phase transformation yielding different crystal phases in situ than observed ex situ. The strong effect of the electron beam and the absence of oxygen is explained by the ability of niobium oxide to form suboxides and accommodate oxygen deficiency via structural strain. While the absence of oxygen yields a crystal phase with similar crystal symmetry like H-Nb_2O_5 and $Nb_3O_7(OH)$ but with different *d*-values, the additional presence of the electron beam features clearly different crystallographic parameters. All together, this study demonstrates the high thermal stability of $Nb_3O_7(OH)$ superstructures related to its crystal structure and morphology. This makes the superstructures especially promising for several functional applications performed at higher temperatures.

ASSOCIATED CONTENT

Supporting Information

The Supporting Information is available free of charge on the ACS Publications website at DOI: 10.1021/acs.cgd.6b00386.

Experimental procedures and additional characterization data, such as XRD pattern, electron diffraction pattern, HRTEM data (PDF)

Movies recorded during heating experiments in situ in the microscope (Movie 1, Movie 2, Movie 3, Movie 4, Movie 5)

AUTHOR INFORMATION

Corresponding Author

*E-mail: c.scheu@mpie.de.

Notes

The authors declare no competing financial interest.

ACKNOWLEDGMENTS

The authors thank the German Research Foundation (DFG) and the Nanosystems Initiative Munich for financial support. The Office of Science, Office of Basic Energy Sciences of the U.S. Department of Energy under Contract No. DE-AC02-05CH11231 supported work at the Molecular Foundry.

REFERENCES

(1) Gatehouse, B.; Wadsley, A. The crystal structure of the high temperature form of niobium pentoxide. *Acta Crystallogr.* **1964**, *17*, 1545.

(2) Kato, K. Structure refinement of H-Nb_2O_5. *Acta Crystallogr., Sect. B: Struct. Crystallogr. Cryst. Chem.* **1976**, *32*, 764.

(3) Kato, K.; Tamura, S. Die Kristallstruktur von T-Nb2O5. *Acta Crystallogr., Sect. B: Struct. Crystallogr. Cryst. Chem.* **1975**, *31*, 673.

(4) Mertin, W.; Andersson, S.; Gruehn, R. Über die Kristallstruktur von M-Nb2O5. *J. Solid State Chem.* **1970**, *1*, 419.

(5) Brauer, G. Die Oxyde des Niobs. *Z. anorg. allg. Chem.* **1941**, *248*, 1.

(6) Vezzoli, G. Electrical properties of NbO2andNb2O5at elevated temperature in air and flowing argon. *Phys. Rev. B: Condens. Matter Mater. Phys.* **1982**, *26*, 3954.

(7) Yamaguchi, O.; Tomihisa, D.; Shirai, M.; Shimizu, K. Formation and Transformation of Solid Solutions in the System Nb_2O_5-Ta_2O_5. *J. Am. Ceram. Soc.* **1988**, *71*, C.

(8) Gruehn, R. Eine weitere neue Modifikation des niobpentoxids. *J. Less-Common Met.* **1966**, *11*, 119.

DOI: 10.1021/acs.cgd.6b00386
Cryst. Growth Des. 2016, 16, 4309−4317

(9) Ercit, T. Refinement of the structure of ?-Nb2O5 and its relationship to the rutile and thoreaulite structures. *Mineral. Petrol.* **1991**, *43*, 217.
(10) Waldron, J.; Green, M.; Neumann, D. Structure and electronic properties of monoclinic Nb12O29. *J. Phys. Chem. Solids* **2004**, *65*, 79.
(11) Goodenough, J.; Hamnett, A.; Huber, G.; Madelung, O.; Hullinger, F.; Leiß, M.; Ramasesha, S.; Werheit, H. *Physics of Non-Tetrahedrally Bonded Binary Compounds III/Physik Der Nicht-tetraedrisch Gebundenen Binären Verbindungen III*; Landolt-Bornstein: Numerical Data and Functional Relationshi; Springer: Berlin, 1984.
(12) Prado, A.; Bolzon, L.; Pedroso, C.; Moura, A.; Costa, L. Nb2O5 as efficient and recyclable photocatalyst for indigo carmine degradation. *Appl. Catal., B* **2008**, *82*, 219.
(13) Lin, H.-Y.; Yang, H.-C.; Wang, W.-L. Synthesis of mesoporous Nb2O5 photocatalysts with Pt, Au, Cu and NiO cocatalyst for water splitting. *Catal. Today* **2011**, *174*, 106.
(14) Zhao, Y.; Zhou, X.; Ye, L.; Tsang, S. Nanostructured Nb_2O_5 catalysts. *Nano Rev.* **2012**, *3*, 1.
(15) Liu, H.; Gao, N.; Liao, M.; Fang, X. Hexagonal-like Nb(2)O(5) nanoplates-based photodetectors and photocatalyst with high performances. *Sci. Rep.* **2015**, *5*, 7716.
(16) Idrees, F.; Cao, C.; Ahmed, R.; Butt, F.; Butt, S.; Tahir, M.; Tanveer, M.; Aslam, I.; Ali, Z. Novel Nano-Flowers of Nb_2O_5 by Template Free Synthesis and Enhanced Photocatalytic Response Under Visible Light. *Sci. Adv. Mater.* **2015**, *7*, 1298.
(17) Cui, H.; Zhu, G.; Xie, Y.; Zhao, W.; Yang, C.; Lin, T.; Gu, H.; Huang, F. Black nanostructured Nb2O5with improved solar absorption and enhanced photoelectrochemical water splitting. *J. Mater. Chem. A* **2015**, *3*, 11830.
(18) Guo, P.; Aegerter, M. RU(II) sensitized Nb2O5 solar cell made by the sol-gel process. *Thin Solid Films* **1999**, *351*, 290.
(19) Lenzmann, F.; Krueger, J.; Burnside, S.; Brooks, K.; Grätzel, M.; Gal, D.; Rühle, S.; Cahen, D. Surface Photovoltage Spectroscopy of Dye-Sensitized Solar Cells with TiO2, Nb2O5, and SrTiO3Nanocrystalline Photoanodes: Indication for Electron Injection from Higher Excited Dye States. *J. Phys. Chem. B* **2001**, *105*, 6347.
(20) Wei, M.; Qi, Z.-m.; Ichihara, M.; Zhou, H. Synthesis of single-crystal niobium pentoxide nanobelts. *Acta Mater.* **2008**, *56*, 2488.
(21) Ghosh, R.; Brennaman, M.; Uher, T.; Ok, M.-R.; Samulski, E.; McNeil, L.; Meyer, T.; Lopez, R. Nanoforest Nb2O5 photoanodes for dye-sensitized solar cells by pulsed laser deposition. *ACS Appl. Mater. Interfaces* **2011**, *3*, 3929.
(22) Izumi, F.; Kodama, H. Hydrothermal Synthesis and Characterization of $Nb_3O_7(OH)$. *Z. Anorg. Allg. Chem.* **1978**, *441*, 196.
(23) Zhang, H.; Wang, Y.; Yang, D.; Li, Y.; Liu, H.; Liu, P.; Wood, B.; Zhao, H. Directly hydrothermal growth of single crystal Nb3O7(OH) nanorod film for high performance dye-sensitized solar cells. *Adv. Mater.* **2012**, *24*, 1598.
(24) Wu, J.; Wang, J.; Li, H.; Xue, D. Solution-phase tailored growth of NB3O7(OH) thin films. *Thin Solid Films* **2013**, *544*, 545.
(25) Betzler, S.; Wisnet, A.; Breitbach, B.; Mitterbauer, C.; Weickert, J.; Schmidt-Mende, L.; Scheu, C. Template-free synthesis of novel, highly-ordered 3D hierarchical Nb3O7(OH) superstructures with semiconductive and photoactive properties. *J. Mater. Chem. A* **2014**, *2*, 12005.
(26) Hmadeh, M.; Hoepfner, V.; Larios, E.; Liao, K.; Jia, J.; Jose-Yacaman, M.; Ozin, G. New Hydrogen-Evolution Heteronanostructured Photocatalysts: Pt-Nb O (OH) and Cu-Nb O (OH). *ChemSusChem* **2014**, *7*, 2104.
(27) Hu, P.; Hou, D.; Wen, Y.; Shan, B.; Chen, C.; Huang, Y.; Hu, X. Self-assembled 3D hierarchical sheaf-like Nb3O7(OH) nanostructures with enhanced photocatalytic activity. *Nanoscale* **2015**, *7*, 1963.
(28) Zhang, H.; Wang, Y.; Liu, P.; Chou, S. L.; Wang, J. Z.; Liu, H.; Wang, G.; Zhao, H. Highly Ordered Single Crystalline Nanowire Array Assembled Three-Dimensional Nb3O7(OH) and Nb2O5 Superstructures for Energy Storage and Conversion Applications. *ACS Nano* **2016**, *10*, 507.
(29) Kofstad, P. Studies of electrical conductivity of Nb2O5 as a function of oxygen pressure at 600−1200°C. *J. Phys. Chem. Solids* **1962**, *23*, 1571.
(30) Dehm, G.; Howe, J.; Zweck, J. *In-Situ Electron Microscopy: Applications in Physics, Chemistry and Materials Science*; Wiley: New York, 2012.
(31) Asoro, M.; Kovar, D.; Ferreira, P. In situ Transmission Electron Microscopy Observations of Sublimation in Silver Nanoparticles. *ACS Nano* **2013**, *7*, 7844.
(32) Oh, S. H.; Kauffmann, Y.; Scheu, C.; Kaplan, W. D.; Rühle, M. Ordered liquid aluminum at the interface with sapphire. *Science* **2005**, *310*, 661.
(33) Oh, S. H.; Chisholm, M. F.; Kauffmann, Y.; Kaplan, W. D.; Luo, W.; Rühle, M.; Scheu, C. Oscillatory mass transport in vapor-liquid-solid growth of sapphire nanowires. *Science* **2010**, *330*, 489.
(34) Agrawal, A.; Cizeron, J.; Colvin, V. In Situ High-Temperature Transmission Electron Microscopy Observations of the Formation of Nanocrystalline TiC from Nanocrystalline Anatase (TiO2). *Microsc. Microanal.* **1998**, *4*, 269.
(35) Yokota, T.; Murayama, M.; Howe, J. Insitu Transmission-Electron-Microscopy Investigation of Melting in Submicron Al-Si Alloy Particles under Electron-Beam Irradiation. *Phys. Rev. Lett.* **2003**, *91*, 265504.
(36) Long, N.; Petford-Long, A. In-situ electron-beam-induced reduction of CuO: A study of phase transformations in cupric oxide. *Ultramicroscopy* **1986**, *20*, 151.
(37) Smith, D.; McCartney, M.; Bursill, L. The electron-beam-induced reduction of transition metal oxide surfaces to metallic lower oxides. *Ultramicroscopy* **1987**, *23*, 299.
(38) Su, D. S.; Wieske, M.; Beckmann, E.; Blume, A.; Mestl, G.; Schlögl, R. Electron Beam Induced Reduction of V_2O_5 Studied by Analytical Electron Microscopy. *Catal. Lett.* **2001**, *75*, 81.
(39) Anderson, J.; Browne, J.; Cheetham, A.; Dreele, R.; Hutchison, J.; Lincoln, F.; Bevan, D.; Straehle, J. Point Defects and Extended Defects in Niobium Oxides. *Nature* **1973**, *243*, 81.
(40) Balachandran, U.; Eror, N. Non-stoichiometric disorder in H-Nb2O5 at elevated temperatures. *J. Mater. Sci.* **1982**, *17*, 1286.
(41) Schilling, O. Thermodynamic properties of nonstoichiometric H-Nb2 O5x derived from a statistical model of its defect structure. *J. Phys. Chem. Solids* **1986**, *47*, 595.
(42) Anderson, J.; Browne, J. M.; Hutchison, J. Electron microscopy of the niobium oxides. I. Twinning and defects in H-Nb2O5. *J. Solid State Chem.* **1972**, *5*, 419.
(43) Shukla, A.; Ercius, P.; Gautam, A.; Cabana, J.; Dahmen, U. Electron Tomography Analysis of Reaction Path during Formation of Nanoporous NiO by Solid State Decomposition. *Cryst. Growth Des.* **2014**, *14*, 2453.
(44) Campbell, F. *Elements of Metallurgy and Engineering Alloys*; ASM International: Materials Park, Ohio, 2008.
(45) Hull, D.; Bacon, D. In *Introduction to Dislocations*, 4th ed.; Hull, D., Bacon, D., Eds.; Butterworth-Heinemann: Oxford, 2001; pp 82−101.
(46) Wu, J.; Jia, C.; Urban, K.; Hao, J.; Xi, X. Microstructure and misfit relaxation in SrTiO3/SrRuO3 bilayer films on LaAlO3(100) substrates. *J. Mater. Res.* **2001**, *16*, 3443−3450.
(47) Jin Fan, H.; Knez, M.; Scholz, R.; Nielsch, K.; Pippel, E.; Hesse, D.; Zacharias, M.; Gösele, U. Monocrystalline spinel nanotube fabrication based on the Kirkendall effect. *Nat. Mater.* **2006**, *5*, 627.
(48) Buscaglia, M.; Buscaglia, V.; Viviani, M.; Dondero, G.; Röhrig, S.; Rüdiger, A.; Nanni, P. Ferroelectric hollow particles obtained by solid-state reaction. *Nanotechnology* **2008**, *19*, 225602.
(49) Dahmen, U.; Kim, M. G.; Searcy, A. W. Microstructural evolution during the decomposition of Mg(OH)2. *Ultramicroscopy* **1987**, *23*, 365.
(50) Tilley, R. *Principles and Applications of Chemical Defects*; Taylor & Francis: New York, 1998.
(51) Egerton, R. *Electron Energy-Loss Spectroscopy in the Electron Microscope*; Springer: New York, 2011.

DOI: 10.1021/acs.cgd.6b00386
Cryst. Growth Des. 2016, 16, 4309−4317

(52) Bach, D.; Störmer, H.; Schneider, R.; Gerthsen, D.; Verbeeck, J. EELS investigations of different niobium oxide phases. *Microsc. Microanal.* **2006**, *12*, 416.
(53) Bach, D.; Schneider, R.; Gerthsen, D.; Verbeeck, J.; Sigle, W. EELS of niobium and stoichiometric niobium-oxide phases—Part I: plasmon and near-edges fine structure. *Microsc. Microanal.* **2009**, *15*, 505.

DOI: 10.1021/acs.cgd.6b00386
Cryst. Growth Des. 2016, 16, 4309−4317